

Polymer Optical Waveguides With GI and W-Shaped Cores for High-Bandwidth-Density On-Board Interconnects

Ryota Kinoshita, Kimio Moriya, Koji Choki, and Takaaki Ishigure, *Member, IEEE*

Abstract—We fabricate polynorbornene-based graded-index (GI) core polymer optical waveguides using the photoaddressing method, and demonstrate that the GI-core polymer waveguides are capable of realizing high-bandwidth-density on-board optical interconnects. Because of the tight optical confinement effect of the parabolic refractive index profile, the fabricated GI-core polymer waveguides exhibit superior optical properties compared to step-index (SI) core polymer waveguides: low propagation loss, low connection loss with GI multimode fiber (MMF) with wide misalignment tolerance, and low interchannel crosstalk even under a small pitch size are experimentally confirmed. Furthermore, interchannel crosstalk due to multicore operation is experimentally evaluated, and a method to estimate the interchannel crosstalk in multimode polymer parallel optical waveguides under multicore operation is proposed for the first time, to the best of our knowledge. The photoaddressing method capable of fabricating even low-loss GI-core polymer waveguide circuits will pave the way for realizing low-cost and high-bandwidth-density optical printed circuit boards.

Index Terms—Graded-index core, interchannel crosstalk, on-board interconnection, optical printed circuit board (O-PCB), photoaddressing method, polymer optical waveguide.

I. INTRODUCTION

WITH the continuous growth of data processing speed in high-performance computers (HPCs), current backplane and on-board interconnections based on electrical wiring have become a bottleneck. For further advancement in next-generation HPCs, optical interconnect technologies realizing low-power consumption, high-density, and low-cost links are drawing much attention. Over the past few decades, parallel multimode optical fiber (MMF) modules have already been deployed in rack-to-rack interconnects in some HPCs with a teraflop to petaflop scales [1]. In the coming decades, exascale computing systems will require on-board, backplanes, and even intrachip optical interconnects, which will provide higher

density wiring with much higher speed transmission while maintaining lower power consumption.

Here, for on-board interconnections, it is anticipated that multimode polymer optical waveguides incorporated with printed circuit boards (PCBs) will be realized, because the large core size of multimode waveguides allows easy connection with other optical components. Hence, optical printed circuit boards (O-PCBs) promise to meet such demands. There have been many reports on O-PCBs particularly utilizing multimode polymer waveguides with step-index (SI) square-shaped cores [2]–[5], and they are mainly applied to 10 Gbps links with a few tens of centimeter waveguide length. However, for O-PCBs in the next generation HPCs, a link distance of 1 m is expected to be covered by polymer waveguide-based links, and the transmission rate of the link should be higher than 20 Gbps [6], [7]. For a 25 Gbps transmission at 850 nm, it has previously been confirmed that maintaining a bit error ratio (BER) of 10^{-12} requires received power as high as -6 dBm [8]. Hence, even in such a short-distance optical link, the link power budget should be limited to at most 10 dB. The propagation loss of current polymer optical waveguides as low as 0.03 dB/cm (the lowest level at 850-nm wavelength) is sufficiently high that extra optical loss, e.g., coupling/connection loss and power penalty due to dispersion, should be as small as possible in the polymer waveguide links. Therefore, we have to optimize polymer waveguide structures and waveguide-based optical links for minimizing the link power budget.

One of our groups at Keio University has experimentally demonstrated the superior optical properties of graded-index (GI)-core polymer optical waveguides, such as low-propagation loss, low interchannel crosstalk, high bandwidth, and high coupling efficiency with MMFs and photodetectors (PDs), compared to conventional SI-core waveguides [9], [10]. In this paper, we introduce a new fabrication method for GI-core polymer optical waveguide: the photoaddressing method utilizing a thermally resistant polynorbornene resin [11], which is developed at Sumitomo Bakelite Company. The experimentally fabricated GI-core polymer waveguides are characterized, and we demonstrate that even GI-square cores of the fabricated waveguides show similar or superior properties to the GI-circular core waveguides we previously reported [10], [12].

In the following sections, first, we discuss the fabrication method for GI-core waveguides. Second, we focus on the connection loss between the polymer waveguides and a GI-MMF, where we focus on a polymer waveguide-based on-board link connected with MMF ribbons.

Manuscript received July 1, 2013; revised August 13, 2013; accepted August 14, 2013. Date of publication September 23, 2013; date of current version November 27, 2013.

R. Kinoshita is with the Keio University, Graduate School of Science and Technology, Yokohama 223-8522, Japan (e-mail: r_k1267@z8.keio.jp).

K. Moriya and K. Choki are with the Sumitomo Bakelite Co., Ltd., Information and Telecommunication Material Laboratories, Utsunomiya, Tochigi 321-3231, Japan (e-mail: k_moriya@sumibe.co.jp; choki@sumibe.co.jp).

T. Ishigure is with the Keio University, Faculty of Science and Technology, Yokohama 223-8522, Japan (e-mail: ishigure@appi.keio.ac.jp).

Color versions of one or more of the figures in this paper are available online at <http://ieeexplore.ieee.org>.

Digital Object Identifier 10.1109/JLT.2013.2279791

Next, we also demonstrate that GI-core polymer waveguides exhibit low interchannel crosstalk, compared to the SI-core counterparts. Here, we discuss about the effects of the small pitch size, the multicore simultaneous operation, and the power of cladding modes. Finally, we show the GI-core polymer optical waveguide fabricated by the photoaddressing method is a promising component for realizing high-bandwidth-density wiring on PCBs.

II. FABRICATION OF GI (W-SHAPED) CORE POLYMER WAVEGUIDE: PHOTOADDRESSING METHOD

Polynorbornene-based SI-core optical waveguides were proposed by Sumitomo Bakelite Co. in 2006, which were fabricated utilizing the photoaddressing technique [11]. Polynorbornene is a cyclic olefin resin with a high refractive index and high temperature resistance. Since polynorbornene is an amorphous (non-crystalline) polymer, it realizes low-scattering loss. Particularly, low optical loss is achieved at a wavelength of 850 nm, which is an emission wavelength of GaAs-based vertical cavity surface emitting lasers (VCSELs) widely utilized in very-short-reach (VSR) optical networks.

Meanwhile, polymer parallel optical waveguides with GI cores have been successfully fabricated using various fabrication methods: preform method [9], [10], soft-lithography method [13] and dispenser method [12], which had been reported by some of the authors. There, the capability of high-bandwidth-density and high-speed parallel optical links has also been demonstrated with GI-core polymer waveguides. In particular, the Mosquito method that utilizes a microdispenser is a method to obtain low-loss and high-bandwidth-density GI-*circular* core polymer waveguides without a photomask; it is therefore very costeffective. In the Mosquito method, waveguide structures are directly written by dispensing a viscous core monomer from a thin needle whose output end remains inserted in a cladding monomer layer. Consequently, the Mosquito method is applicable to a waveguide with isolated channel structures, while it would be difficult for the Mosquito method to draw circuit structures that would involve couplers, splitters, and crossed cores. Hence, we focus on the polynorbornene waveguides which can form graded refractive index profiles in the cores by modifying the photoaddressing method.

The photoaddressing method is schematically shown in Fig. 1. Fig. 1(a) shows the original fabrication technique of polynorbornene-based SI-square core polymer waveguides. First, the precursor for the cores is coated on a substrate using the doctor-blade technique. The coated layer is prebaked followed by a UV exposure through a photomask. The coated layer includes a monomer and photoinitiator. The curing reaction after the UV exposure under a high-temperature atmosphere turns the UV-exposed area into a cladding with a low refractive index ($n = 1.53$) due to selective cross-linking reactions at the UV-exposed area. On the other hand, the area protected by the photomask has a higher refractive index ($n = 1.55$), forming the waveguide cores. Next, the patterned film is laminated between two cladding films having a uniform refractive index of 1.52 to obtain an SI-square core waveguide, as shown in Fig. 1(a). Here,

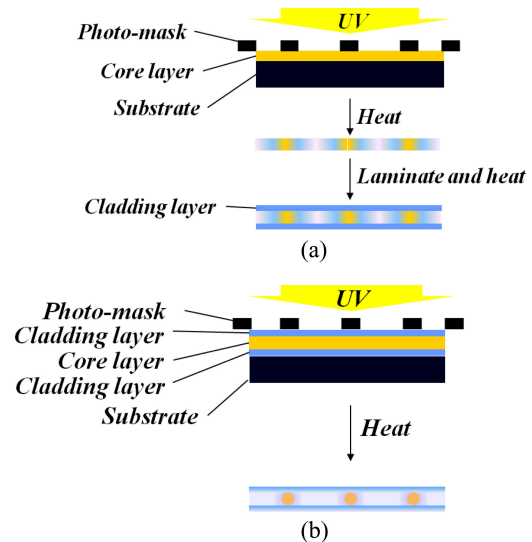


Fig. 1. Fabrication technique of the photoaddressing method for (a) SI-core and (b) GI-core waveguide.

by adjusting the curing condition, a concentration distribution of the high-index polymer is formed in the horizontal direction due to the monomer diffusion, which corresponds to the refractive index profile in the horizontal direction [14]. Hence, the index profile in the horizontal direction can be varied from SI to parabolic (GI). Contrastingly, the index profile in the vertical direction is fixed to be an SI profile.

Meanwhile, a fabrication method of GI-cores (in both horizontal and vertical directions) is shown in Fig. 1(b). The precursors for core and claddings are prepared and coated onto a substrate one by one. Various kinds of refractive index modifiers can be incorporated in the precursor prior to use. The coated layers are prebaked and exposed to a UV light through a photomask to obtain a waveguide, as well. Here, the index modifiers added to the precursor contribute to the formation of an index profile in the vertical direction.

Thus, in this method, the fabrication process is much simpler than the method of Fig. 1(a). In this paper, we mainly focus on the GI-core waveguides fabricated using the method of Fig. 1(b).

III. OPTICAL PROPERTIES

A. Refractive Index Profile

For forming GI-*circular* cores in planer waveguides, the preform method was adopted first [10]. Next, in order to utilize 3-D cross-linkable polymer materials, the dispenser method was developed [12]. Compared to those two methods, the polynorbornene-based waveguides fabricated using the photoaddressing method have GI-*square*-cores. The index profiles formed in the cores are evaluated. Fig. 2 shows the results of the refractive index profile measurement in a GI-core waveguide. As observed in Fig. 2(a), clear concentric interference fringe patterns are observed in all the cores, which is similar to the case of GI-*circular* cores [10], [12]. It is noted that although the outer core shape is square, the fringe patterns are concentric circular shapes, which means a centrosymmetric near-parabolic

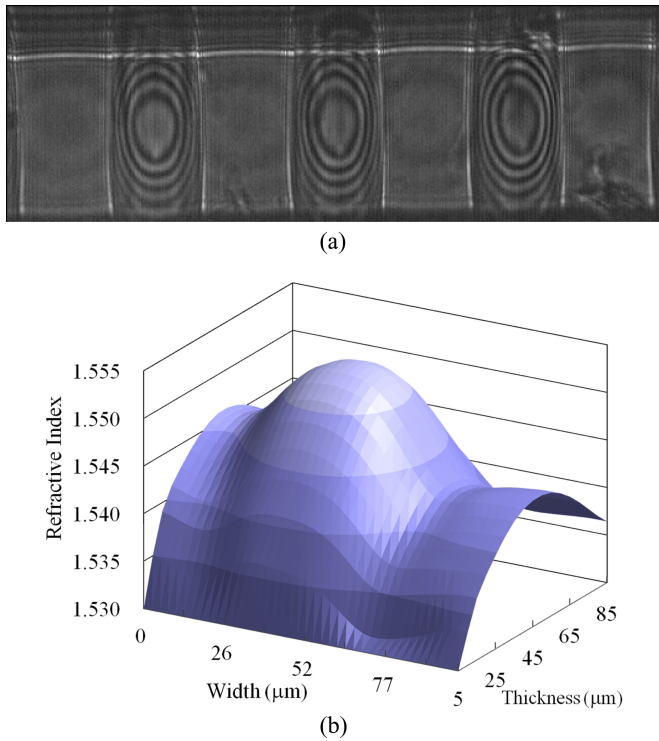


Fig. 2. (a) Interference fringe pattern and (b) refractive index profile calculated for one core of the waveguide from the fringe pattern in Fig. 2(a).

refractive index profile is formed in the core region. Indeed, a near-parabolic refractive index profile is confirmed by calculating the profile from the fringe pattern, as shown in Fig. 2(b). The obtained profiles in the horizontal and vertical directions in Fig. 2(b) were fitted to a well-known power-law equation expressed by (1), and the best-fit index exponent g in both directions is 2.5 on average

$$n(r) = n_1 \left[1 - 2\Delta \left(\frac{r}{a} \right)^g \right]^{1/2} \quad (0 \leq r \leq a) \quad (1)$$

$$\Delta = \frac{n_1^2 - n_2^2}{2n_1^2} \cong \frac{n_1 - n_2}{n_1} \quad (2)$$

where r is the distance from the core center to the measured point, n_1 and n_2 are the refractive indexes at the core center ($r = 0$) and the cladding, respectively, a is the half width of the core for the square core, and g is the index exponent. In Fig. 2, it is noteworthy that the index profile in the horizontal direction (in the width axis) has a trench outside the parabolic distribution, making it resemble a W-shaped profile. This index trench could be formed due to the monomer diffusion in the photoaddressing method. We have already confirmed that W-shape profiles decrease the interchannel crosstalk in parallel waveguides compared to GI-core one [15], [16]. Hence, automatic index trench formation is preferable from the interchannel crosstalk point of view.

From the index profile and far-field pattern (FFP) measurement, the numerical aperture (NA) of the GI polymer waveguide is calculated to be between 0.19–0.23. The NA of the GI-core waveguide is lower than the NA of the general SI-core

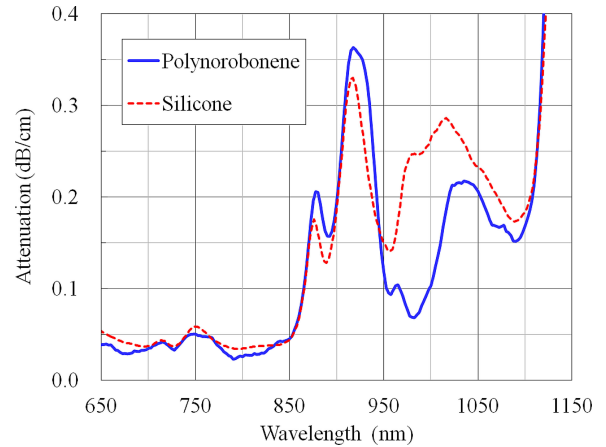


Fig. 3. Loss spectrum of polynorbornene- and silicone-based waveguides.

waveguides (~ 0.3). However, since a waveguide link connected with silica-based MMF is a primary goal in this paper, the NA of the waveguides should be the same as that of MMF (0.21) for a low-connection loss.

B. Propagation Loss Spectrum

The propagation loss of a GI-square core waveguide fabricated by the photoaddressing method is measured using the cut-back method. In this measurement, a halogen–tungsten lamp (white light source) was used, and a 1-m long, 50- $\mu\text{m}\phi$ core GI-MMF worked as a launching probe to couple the light into a channel of the waveguide. A 1-m long, 100- $\mu\text{m}\phi$ core SI-MMF probe whose NA (0.29) is higher than the NA of the waveguide was used to collect all the output light from the channel of the waveguide and guide it to an optical spectrum analyzer. We used a standard dicing saw for cutting the waveguide, and a 20-cm long waveguide was evaluated, which should be long enough to accurately detect the optical power variation before and after dicing the waveguide.

The obtained propagation loss spectrum is shown in Fig. 3. From the spectrum, the propagation loss of the waveguide at 850 nm is found to be 0.0457 dB/cm, which is almost the same as or slightly less than the loss of SI-core polynorbornene-based waveguides [11]. For comparison, the loss spectrum of a GI-circular core silicone-based waveguide fabricated using the Mosquito method [12] is also shown in Fig. 3. The propagation loss at 850 nm is almost the same, while it is very interesting that the loss in a wavelength range from 950 to 1110 nm is slightly lower compared to the silicone-based waveguide. This difference is attributed to the absorption loss dependence of C-H bonds on the chemical structure.

C. Waveguide-Based on-Board Link Configuration

Enormous efforts have been focused on realizing point-to-point polymer optical waveguide links [2]–[6], where a polymer optical waveguide directly connects a light source and a photodetector. In this case, the length of the polymer waveguide is at most 15 to 20 cm. Contrastingly, multimode fiber links that were originally deployed for rack-to-rack interconnects are now

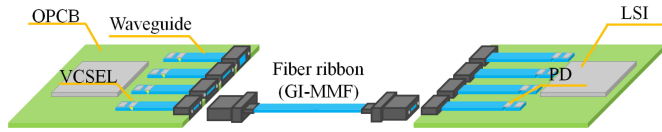


Fig. 4. Configuration of inter O-PCB link model composed of two polymer waveguides and a multimode fiber.

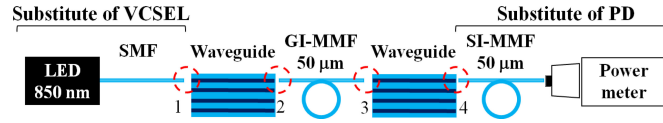


Fig. 5. Experimental setup of connection loss measurement.

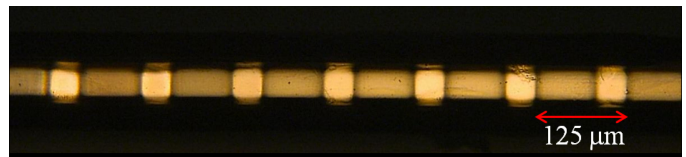
expected to be extended as close to the processing chips as possible in order to minimize the signal distortion of the metal wirings on PCBs [17]. That means signal conversions from electrical to optical and vice versa should be carried out very close to the chips. On the other hand, O-PCB technologies would be another solution to realize well-organized optical wirings on-board. In this case, polymer optical waveguides on PCBs would be required to have a direct connection to GI-MMFs with a $50\text{-}\mu\text{m}$ circular core at the edge of PCBs. Hence, in this paper, we focus on an O-PCB link comprised of two polymer waveguides (supposed to be integrated on PCBs) connected by GI-core MMF ribbons, as shown in Fig. 4. For simplification, only a unidirectional link is drawn in Fig. 4, but a bidirectional link is realized with this link model using multichannel waveguides.

Here, the connections of these different transmission channels are of concern, because it could cause connection losses. At the connection points, mode profile mismatch and light leakage due to different core shapes and sizes could cause connection loss. On the other hand, the polymer optical waveguides with GI cores we have developed exhibit a tight optical confinement at the core center [18]. Furthermore, the waveguide structure of the GI-core waveguide is almost the same as that of the GI-MMF. Therefore, it is expected that the connection loss between the GI-MMF and the waveguide with the GI-core is lower than the connection loss between the GI-MMF and the SI-core waveguide.

Hence, in the next section, we focus on the connection point between multimode waveguides with different structures and the GI-MMF, and then, demonstrate how GI-core waveguides are advantageous for integrating them on PCBs.

D. Connection Loss With MMF

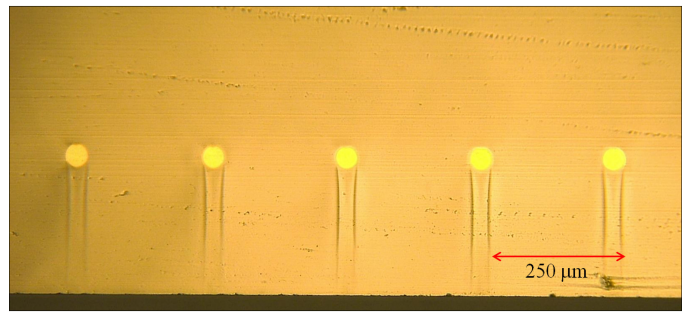
In the waveguide link model illustrated in Fig. 4, each connection of composing components is numbered from connection point 1 to 4, as shown in Fig. 5. With an LED light source at a wavelength of 850 nm , we used a single-mode fiber (SMF) satisfying the single-mode condition at 850 nm as a launching probe. The SMF has almost the same spot size as the size ($\sim 10\text{ }\mu\text{m}$) of the active areas of VCSELs. In the actual O-PCB models in Fig. 4, the lightwave emitted from a VCSEL is normally coupled to a polymer waveguide integrated on PCB via a 45° mirror (not shown in Fig. 4). Hence, a gap of tens of microns could exist between the VCSEL and the waveguide (as an optical via), and the



(a)



(b)



(c)

Fig. 6. (a) Cross section of 11-channel polymer parallel optical waveguide with $40\text{ }\mu\text{m} \times 40\text{ }\mu\text{m}$ GI-square-cores and with a $125\text{-}\mu\text{m}$ pitch (b) Cross section of 12-channel polymer parallel optical waveguide with $40\text{ }\mu\text{m} \times 40\text{ }\mu\text{m}$ SI-square-cores with a $250\text{-}\mu\text{m}$ pitch (c) Cross section of 12-channel polymer parallel optical waveguide with $40\text{-}\mu\text{m}\varnothing$ GI-circular-cores and with a $250\text{-}\mu\text{m}$ pitch.

emitted beam could diverge during the free-space propagation in the optical via. Here, the beam divergence angle and the number of transverse modes from the VCSELs depend on the bias current and structure of the VCSELs. Therefore, it is difficult to experimentally establish a reproducible launching condition when we use a VCSEL chip for the light source. Hence, in the test setup, first the light was coupled to the waveguide via a 1-m SMF probe. We also used a $50\text{-}\mu\text{m}\varnothing$ MMF with an SI-circular core as a detection probe, substituting for a $50\text{-}\mu\text{m}\varnothing$ photodiode. For the waveguide to be evaluated, polynorborene-based GI-core waveguides were utilized while conventional SI-core and GI-circular core waveguides with the same core size as the polynorborene-based one were also evaluated for comparison. The cross sections of all the waveguides tested here are shown in Fig. 6. As shown in Fig. 6, the waveguides for comparison have a $250\text{-}\mu\text{m}$ pitch.

The loss at each connection point (1 to 4) is estimated by measuring the insertion loss of the waveguides. The output power from the waveguides and fibers were detected using an optical power-meter (ANDO AQ-2140 & AQ-2741) which has an active area sufficiently larger than the core sizes of the waveguides and fibers. The connection loss at connection point 2 (connection from the waveguide to the GI-MMF) is calculated from the difference of the two adjacent output powers.

The measured insertion losses are summarized in Table I, when the waveguides and MMFs are perfectly aligned with no air-gap and no misalignment. Since the waveguide and MMF were just butt-coupled, no physical contact is realized at the connection, such that a slight air-gap might be involved. In many

TABLE I
INSERTION LOSS OF WAVEGUIDES

	1-3	3-5	Total
GI square (70-mm long)	1.29 dB	1.32 dB	2.61 dB
GI circular (50-mm long)	1.58 dB	1.84 dB	3.42 dB
SI square (50-mm long)	1.72 dB	2.29 dB	4.01 dB

TABLE II
CONNECTION LOSS AT CONNECTION POINT

	2	3
GI square (70-mm long)	0.41 dB	0.44 dB
GI circular (50-mm long)	0.77 dB	0.46 dB
SI square (50-mm long)	0.73 dB	0.73 dB

previous reports, matching oils were often used at the connection points for reducing the Fresnel reflection, but it would not be realistic to use such fluids in actual on-board interconnect applications. Therefore, we did not use matching oils in this measurement. The waveguides tested here have different waveguide lengths. Therefore, it is difficult to directly compare the measured insertion loss values shown in Table I, although it is noteworthy that the GI-square core waveguide link shows the lowest insertion loss despite the largest waveguide length. The propagation loss of the GI-square core waveguide is measured to be 0.06 dB/cm using the cut-back method, starting with a 20-cm long waveguide, while it is measured to be 0.045 dB/cm for the GI-circular core waveguide using a 15-cm long waveguide. The value of 0.045 dB/cm at 850 nm is used as the loss of the SI-rectangular core waveguide, which was confirmed by the supplier of the waveguide sample (ADEKA Corporation). The losses for 7-cm (GI-square core waveguide) and 5-cm long waveguides (GI-circular and SI-square core waveguides) are calculated to be 0.42, 0.23, and 0.23 dB, respectively. Therefore, the connection loss is separated from the insertion loss. Total connection losses are estimated from the loss values shown in Table I: the loss difference between the total insertion loss in Table I and the propagation loss of the two waveguides ($0.06 \text{ dB/cm} \times 7 \text{ cm} \times 2$ in the case of GI-square core waveguide). The connection loss at connection points 2 and 3 is summarized in Table II. The connection losses shown here are the averages for 11 or 12 channels in the corresponding waveguides. Then, the total connection losses between connection points 1 to 4 in the links are calculated as 1.77 dB for the GI square-core waveguide link and 2.97 dB for the GI circular-core waveguide link, while it increases to 3.56 dB for the SI-core waveguide.

The near-field patterns (NFPs) measured at connection point 2 are shown in Fig. 7. In the SI-core waveguide, the light in-

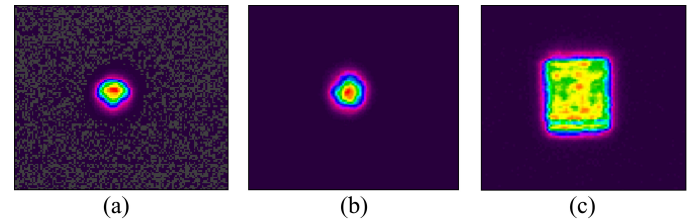


Fig. 7. Near field patterns (NFPs) of the waveguides with (a) GI-square-, (b) GI-circular- and (c) SI-square core at connection point 2.

tensity distribution from the waveguide is uniform in the entire core, despite the circular launch beam with a spot diameter of $10 \mu\text{m}$ from the SMF. Meanwhile, in the GI-core waveguide link, strong light confinement is observed at the core center, which is independent of the outer core shape. This NFP difference leads to the lower connection loss (0.41 dB) of the GI square-core waveguide than that of the SI-core waveguide (0.73 dB) at connection point 2. Therefore, the light confinement effect of the GI-core polymer waveguide is sufficient to show the low connection loss at connection point 2 even if the outer core shape is square. On the other hand, the connection loss (0.77 dB) of GI circular-core is as large as the SI-core waveguide. The reason could be the strong mode conversion from low-order to high-order modes in the GI-circular core polymer waveguide. This seems to be a specific feature of polymer optical waveguides due to intrinsic scattering loss introduced by the dispenser method. Meanwhile, at connection point 3, the both GI-core waveguides show almost the same and lower connection loss compared to the SI-core waveguide. This higher connection loss in the SI-core waveguide is attributed to the mode-field mismatch between the GI- and SI-profiles.

When a matching oil ($n = 1.508$) is used at connection point II of a GI-square core waveguide and a GI-MMF, a connection loss of 0.22 dB is observed. This value is slightly higher than the theoretically calculated loss in which the Fresnel reflection is excluded. This is because of a slight mode-field mismatch. When this loss value is applied to all the connection points, it is expected that approximately 2-dB loss reduction would be attained in the total connection loss when the matching oil is used.

E. Misalignment Tolerance

Fig. 8 shows the misalignment tolerance at connection points from 1 to 4. In this misalignment tolerance measurement, we visually confirmed that the ends of waveguides and fibers are in contact using a microscope. As mentioned earlier, we did not utilize matching oils at each connection point in this measurement as well.

At connection point 1, the misalignment tolerance curve of the SI-core waveguide is wider than that of the GI-circular core. One of the reasons for the narrow tolerance in the GI-circular core waveguide could be the local NA of the GI-core. Increasing the offset amount at connection point 1 gradually decreases the local NA of the GI-core waveguide, and eventually it could be lower than the launching NA, causing connection loss. Another

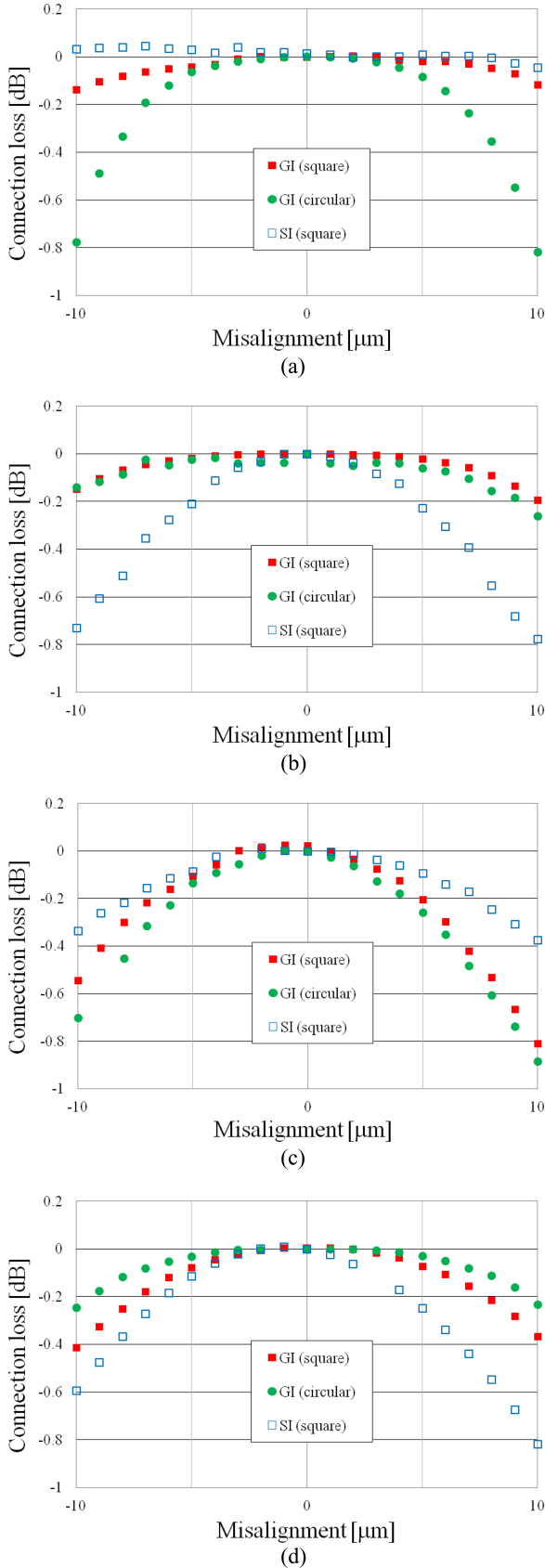


Fig. 8. Misalignment tolerance curve at connection point (a) 1 (b) 2 (c) 3 (d) 4 in the setup shown in Fig. 5.

reason for the small tolerance could be higher loss of high-order modes in the GI-circular core waveguide. This latter possibility seems most likely, because the GI-square core exhibits almost the same alignment curve as the SI-square core, despite having a similar local NA characteristic.

For connection point 1, in actual O-PCBs, in many cases, microlens arrays are used between the light source and waveguide in order to reduce the coupling loss, since the coupling loss without lens system can be devastating. Hence, the connection loss and misalignment tolerance in the GI-core waveguide at connection point 1 shown in Fig. 8(a) could not be problematic.

At connection point 2, the uniform output optical power from the SI square-core, as shown in Fig. 7(c), leads to the narrow misalignment tolerance shown in Fig. 8(b) compared to that of GI-core waveguides. On the contrary, it is noteworthy that the GI-core waveguides exhibit larger misalignment tolerance. For a 1-dB loss tolerance, the misalignment of the GI square and circular core are 33 and 34 μm , respectively, while it decreases to 23 μm for the SI-square core. These results are attributed to the output NFP from the GI-core waveguides at connection point 2: they are much smaller than that from the SI-core waveguide, as shown in Fig. 7. Furthermore, we emphasize that the misalignment tolerances of the GI-core waveguides are independent of the outer core shape.

At connection point 3, since the output NFP from the 50- $\mu\text{m}\phi$ GI-MMF is also confined at the core center due to a parabolic index profile, the SI-core waveguide shows larger misalignment tolerance than the GI-core waveguides, similar to the misalignment curves at connection point 1. However, because the spot size from the GI-MMF is slightly wider than that from the SMF probe at connection point 1, the misalignment tolerances at connection point 3 degrade slightly compared to those at connection point 1.

For the connection to the SI-MMF (proxy for a PD with a 50- $\mu\text{m}\phi$ active area) at connection point 4, similar to connection point 2, the GI-core waveguides exhibit larger misalignment tolerance than the SI-waveguide. For further high-speed data transmission, the optical link requires a smaller PD diameter, which has smaller parasitic capacitance. Therefore, GI-core waveguides would be suitable for the connection to PD with a small active area compared to SI-core waveguides.

Table III summarizes the loss values found from Fig. 8 (a) to (d), when a lateral misalignment of 5 μm is added at each connection point as the worst case. The total connection losses in the GI- and SI-core waveguides increase to approximately 0.29, 0.34, and 0.49 dB, respectively. Hence, if we allow 5- μm misalignment at all the connections, the loss due to the connection in GI-square, GI-circular, and SI-square core waveguide links are simply calculated to be 2.06, 3.31, and 4.05 dB, respectively. Approximately 2-dB connection loss benefit is available in the GI-square core waveguide link over its SI-core counterpart.

F. Direct VCSEL Coupling

In Section III-E, we used an SMF probe with an approximately 10- μm core diameter as a proxy for a VCSEL chip

TABLE III
CONNECTION LOSSES WHEN A 5-MICROMETER LATERAL
MISALIGNMENT IS ADDED

Point	GI square	GI circular	SI square
1	0.04 dB	0.07 dB	0.00 dB
2	0.02 dB	0.04 dB	0.22 dB
3	0.16 dB	0.20 dB	0.09 dB
4	0.07 dB	0.03 dB	0.18 dB
Total	0.29 dB	0.34 dB	0.49 dB

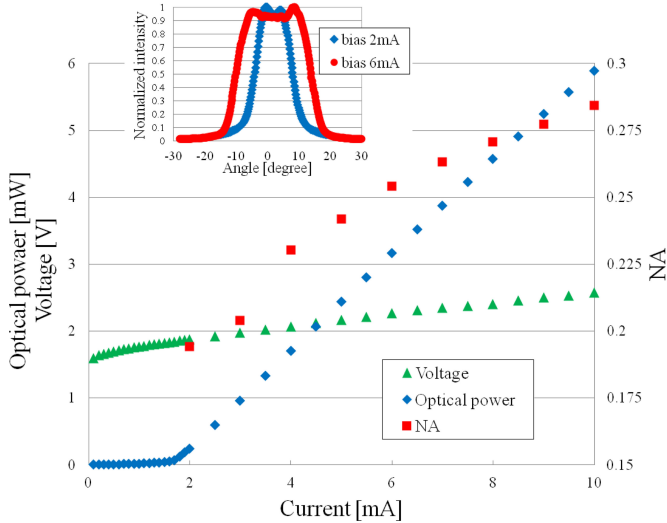


Fig. 9. $L-I-V$ curve of the VCSEL chip adopted for the measurement in addition to the bias current dependence of emitted beam NA (inset) FFPs of the VCSEL chip with bias currents of 2 and 6 mA.

for obtaining a reproducible launching condition of multimode waveguides. In this section, we use a commercially available VCSEL chip emitting at 850 nm. As mentioned previously, the beam divergence angle and the number of transverse modes from VCSELs depend on the bias current and the structure of VCSELs. For optical link applications, the bias current of VCSEL tends to increase in order to ensure sufficient link power budget. However, the beam divergence angles from highly biased VCSELs are generally as wide as 17.5° , corresponding to an NA of 0.3. Even if the chip size is as small as $10\ \mu\text{m}$, such a divergent output beam strongly influences the coupling loss to waveguides. Hence, we should take the bias current of VCSEL into account for estimating the coupling loss.

Here, we select two different bias currents, 2 mA which is close to the threshold current (1.6 mA), and 6 mA which allows to emit sufficiently high output power. Fig. 9 shows the measured $L-I-V$ curve of the VCSEL chip adopted for the measurement. In addition, in the inset of Fig. 9, the measured FFPs of the VCSEL chip with bias currents of 2 and 6 mA are also shown. In Fig. 9, the bias current dependence of the NA of VCSEL beam is also plotted. The NA increases from 0.20 to 0.26 as the current changes from 2 to 6 mA. Furthermore, the angular distribution under 6-mA bias clearly shows double peaks at $\pm 10^\circ$. Hence, highly biased VCSELs can selectively couple

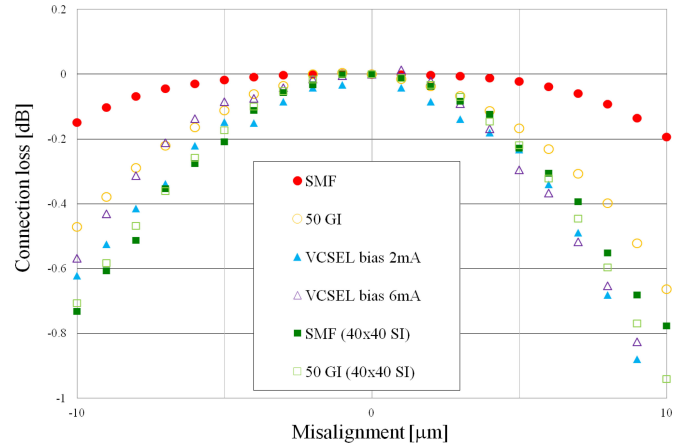


Fig. 10. Comparison of misalignment tolerance of the GI square-core and SI-square core waveguides at connection point 2 under various launching condition of connection point 1.

higher power to the high-order modes of waveguides and fibers, so that the launch condition could be largely different from that using an SMF probe shown in Section III-E.

In this measurement, the VCSEL was butt-coupled to the waveguides with GI square-core and the connection loss and misalignment tolerance at connection point 2 were measured. Due to the bonded metal wire, the core of the waveguide could not be in contact with the VCSEL chip, and thus an approximately $10\text{-}\mu\text{m}$ gap existed between the chip and core. Observations of the connection point via a microscope made it possible to maintain the same gap width throughout the measurement. The results of the GI-square core waveguide are shown in Fig. 10. The misalignment tolerance in the case of 2-mA-biased VCSEL is almost the same as that of 6-mA bias, although a degradation of the tolerance curve is clearly observed compared to that using an SMF launch probe. The reason the misalignment curve is independent of the bias current is because the launch NA of 0.2 under 2-mA bias is high enough to realize an overfilled launching condition within the waveguide ($\text{NA} = 0.19\text{--}0.23$). Thus, we can say the misalignment tolerance of the GI-core waveguide at connection point 2 (GI-GI connection) could be very sensitive to the launch NA as well as the launching spot size at connection point 1.

On the other hand, the misalignment tolerance of the SI-core waveguide link at connection point 2 is independent of the launching condition at connection point 1. Furthermore, the misalignment tolerance of the SI-core waveguide is almost the same or rather narrower than the worst case of the GI-core waveguide, direct coupling to the VCSEL with 6-mA bias. These results indicate that if a restricted mode launch (RML) condition similar to the one for GI-MMF VSR networks, such as 10 Gb Ethernet [19] is applied to the GI-core waveguide links in actual O-PCB applications (using microlens arrays etc.), low connection losses between the waveguide and MMF could be maintained, even if a slight amount of misalignment ($\sim 5\ \mu\text{m}$) is caused at the connection points. Meanwhile, the launch condition does not contribute to reducing the connection loss between the SI-core waveguides and the GI-MMF.

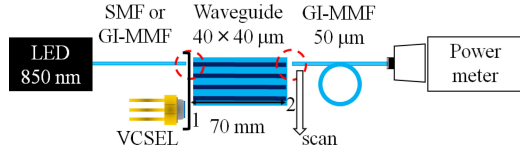


Fig. 11. Experimental setup for measuring crosstalk.

G. Interchannel Crosstalk

We already showed the potential of low interchannel crosstalk in GI-core polymer waveguides even under very narrow pitch [20]. Actually, we simulated how we can decrease the intercore pitch while maintaining an interchannel crosstalk lower than -20 dB for both GI and SI cores. Then, we showed that the minimum pitch of GI-core waveguides could be smaller than that of SI-core waveguides.

Here, conventional SI-core polymer waveguides generally have had a pitch of $250 \mu\text{m}$, while in order to realize higher density wirings, recently, it tends to decrease to $62.5 \mu\text{m}$ or less [6]. One of the concerns in reducing the pitch is an increase in interchannel crosstalk. Therefore, we experimentally compare the crosstalk of the GI square-core waveguides with different pitches: 62.5 , 125 , and $250 \mu\text{m}$ (the core size is $40 \times 40 \mu\text{m}$), which are excited via a $50\text{-}\mu\text{m}\varnothing$ GI-MMF probe, while direct coupling with the VCSEL shown in Fig. 9 under 2 and 6-mA bias currents is also adopted for comparison. The interchannel crosstalk is measured using the setup schematically shown in Fig. 11. First, we measure the output power from the excited core after transmitting a 7-cm long waveguide. The tested waveguides have 11 channels aligned parallel, so that the edge core is excited via a launching probe or via direct coupling with a VCSEL chip. Next, as shown in Fig. 11, the detection probe (GI-MMF) butt-coupled to the output facet of the waveguide is scanned horizontally with a step of $1 \mu\text{m}$ for detecting the output power from the other ten cores, as well as the output from the cladding area.

Fig. 12(a) and (b) are the measured results. From Fig. 12, the GI-core waveguides show sufficiently low (less than -25 dB) interchannel crosstalk except for the one with narrowest pitch ($62.5 \mu\text{m}$) even if the optical power is coupled to the high-order modes by butt-coupled to a highly biased VCSEL chip (overfilled launch).

In addition, it is found from Fig. 12(a) that the interchannel crosstalk depends on the launching condition. When the waveguide is directly connected to the VCSEL chip, although the light emitting area (spot size) is almost the same, the different launching NA depending on the bias current influences the crosstalk. Meanwhile in the case of a $50\text{-}\mu\text{m}\varnothing$ GI-MMF launch probe, although the spot size is wider than that of the VCSEL chip, the launch NA is about 0.2, which is almost the same as that of 2-mA biased VCSEL. Hence, the crosstalk values when coupled to the 2-mA biased VCSEL are almost the same as that excited via the $50\text{-}\mu\text{m}\varnothing$ GI-MMF launch probe. However, even in the worst case in Fig. 12(a), a crosstalk value of less than -20 dB is maintained.

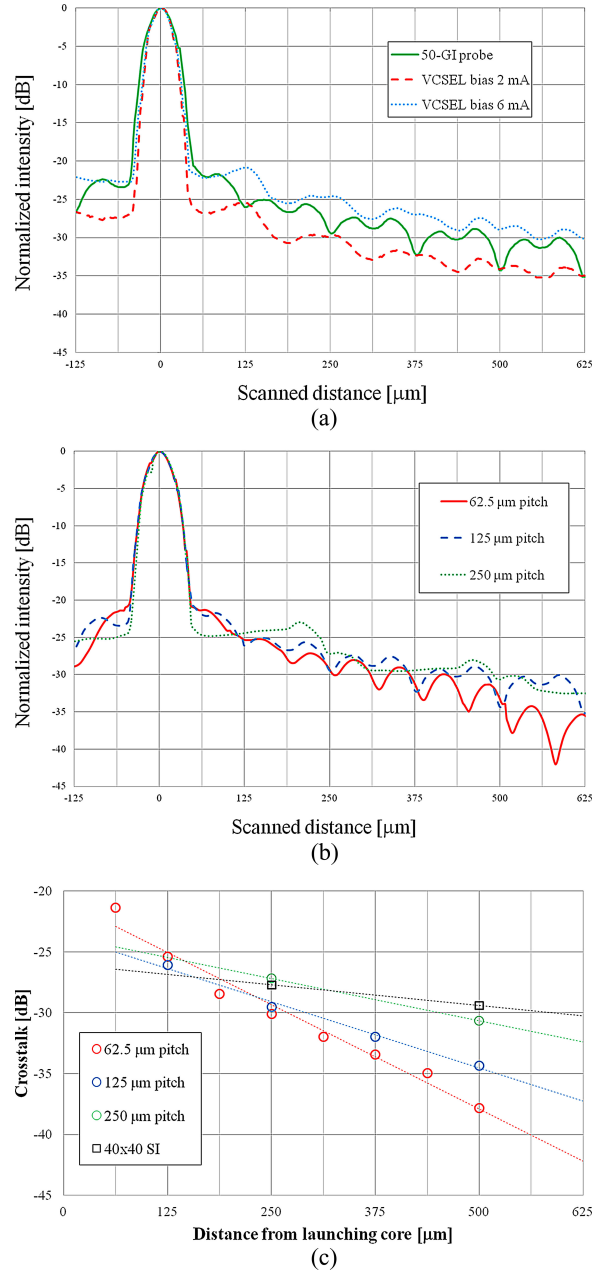


Fig. 12. (a) Interchannel crosstalk measurement results of the GI-core waveguide with a $125\text{-}\mu\text{m}$ pitch excited via a $50\text{-}\mu\text{m}\varnothing$ MMF and VCSEL under bias currents of 2 and 6 mA. (b) Interchannel crosstalk measurement results of the GI-core waveguide with 250- , 125- and $62.5\text{-}\mu\text{m}$ pitch excited via a $50\text{-}\mu\text{m}\varnothing$ GI-MMF. (c) Relationship between the interchannel crosstalk value and the intercore distance.

In Fig. 12(b), the crosstalk values to the nearest channel are found to be -21.34 , -26.05 , and -27.18 dB for 62.5- , 125- , and $250\text{-}\mu\text{m}$ pitch GI-core waveguides, respectively. These crosstalk values in a range from -20 to -28 dB may not sufficiently be low. One reason for the relatively high crosstalk could be the spot size of the launch beam from the $50\text{-}\mu\text{m}\varnothing$ GI-MMF for $40 \mu\text{m} \times 40 \mu\text{m}$ core of the waveguide: the light uncoupled to the waveguide core from the GI-MMF probe remains in the cladding as the cladding modes to increase the interchannel crosstalk.

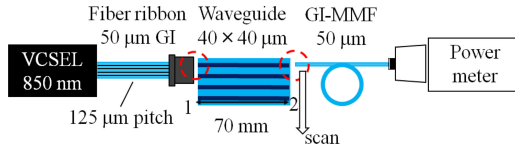


Fig. 13. Experimental setup for measuring crosstalk.

From the results in Fig. 12(b), the relationships between the crosstalk values to each core and the distance between the corresponding two cores are extracted for the three waveguides with different pitches, and they are plotted in Fig. 12(c). From Fig. 12(c), it is found that the crosstalk values almost linearly decrease with respect to the intercore distance, as approximated by the dotted lines. The best-fit lines show the slope values of -0.014 , -0.022 , and -0.034 dB/ μm for the waveguides with 250, 125, and 62.5 μm pitch, respectively, while the slope of 40 $\mu\text{m} \times 40$ μm SI-core (250 - μm pitch) is calculated to be -0.006 dB/ μm . In the GI-core waveguide, the slope is steeper with decreasing pitch size. This pitch dependence of the slope could be explained by the core density (per length): densely aligned cores (narrow pitch) make it more likely for cladding modes to recouple to the cores, and consequently less optical power within cladding modes remains for remote cores. Although such a pitch dependence of crosstalk is seen in Fig. 12(c), we can also find from Fig. 12(c) that there is little waveguide structural dependence: i.e., index profile, particularly in the waveguides with a 250 - μm pitch. This would be due to high power remaining in the cladding (cladding modes) in both waveguides. However, the slope in Fig. 12(c) of the GI-core waveguide is slightly steeper than that of the SI-core waveguide, which could also be influenced by the remaining cladding-mode power. Therefore, the effect of the cladding modes on crosstalk is discussed in detail in the next section.

In actual optical links, the signal light propagates through all or most of the parallel channels of polymer waveguides simultaneously. Hence, it is important that how the interchannel crosstalk is affected by multichannel operation. Although there have been several reports [5], [21] on the measured interchannel crosstalk in polymer waveguides when only one channel is excited, as far as we know, few reports on the crosstalk due to the multichannel operation are available. Therefore, we investigate the crosstalk not only from one excited channel but also from multiple excited cores. For this evaluation, the crosstalk of the GI square-core waveguides was measured by launching multiple cores via a 1-m long, 12-channel, 50 - μm GI-MMF ribbon with a 125 - μm pitch (supplied by Furukawa Electric Company). The measurement setup is schematically shown in Fig. 13. Since each channel of the 12-channel MMF ribbon is connected to 12 different VCSEL sources independently, desired channels are excited.

Fig. 14 summarizes the evaluation scheme of the interchannel crosstalk in the 125 - μm pitch GI-square core polymer waveguide. Since the tested waveguide has 11 channels aligned in parallel, these channels are numbered from channel 1 to channel 11, and then the crosstalk variation to channel 4 (red-colored in Fig. 14) is measured by operating multiple channels as well

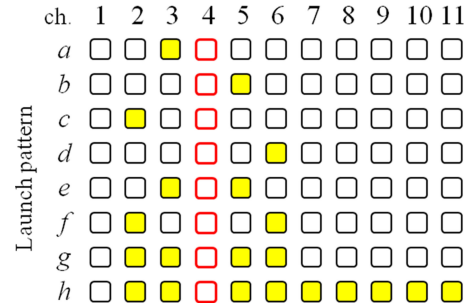


Fig. 14. Various launch patterns for crosstalk measurement due to multicore operation.

TABLE IV
OUTPUT POWER FROM EACH CHANNEL IN VARIOUS LAUNCH PATTERNS

ch.	1	2	3	4	5	6	7-11
<i>a</i>	-	-	-11.36	-38.13	-	-	-
<i>b</i>	-	-	-	-37.45	-11.16	-	-
<i>c</i>	-	-12.98	-	-42.70	-	-	-
<i>d</i>	-	-	-	-40.96	-	-12.77	-
<i>e</i>	-	-	-10.80	-34.31	-10.85	-	-
<i>f</i>	-	-11.94	-	-38.35	-	-12.72	-
<i>g</i>	-	-11.70	-11.02	-32.55	-10.54	-12.74	-
<i>h</i>	-	-11.70	-10.86	-31.61	-10.54	-12.61	-

(dBm).

as single-channel operation, under separate conditions *a* to *h*, as indicated in Fig. 14. Here, the channels with yellow color transmit optical signals.

The measured output power from each channel is summarized in Table IV, with the output power from the excited channel(s) with yellow color. In Table IV, dash (-) means we did not measure the output power data for those channels, while the output power only from channel 4 is focused. Since the output power from each channel of MMF ribbon is not necessarily uniform, and the coupling efficiencies to channel 2 to channel 11 are also varied, the output power from the excited channels is in a range from -10.5 to -13 dBm, as indicated in Table IV (with gray color).

From Table IV, it is obvious that the crosstalk values from the second nearest cores (channel 2 and channel 6 for channel 4) are not negligible as in the pattern *c*, *d* and *f*, although the crosstalk value is strongly dependent on the intercore distance. From Fig. 12(c), we find a linear relationship between the crosstalk from arbitrary channel *N* to channel 4, expressed as XT_{N-4} , and the distance between channel *N* and channel 4 (x_{N-4}) in the 125 - μm pitch GI-core waveguide, which is described as follows:

$$XT_{N-4}(\text{dB}) = -0.0218 \times x_{N-4}(\mu\text{m}) - 23.634. \quad (3)$$

Therefore, when channel *N* is excited and the output power from channel *N* is P_N in dBm, the output power from unexcited channel 4 due to the crosstalk from channel *N*, ($P_4(XT_{N-4})$)

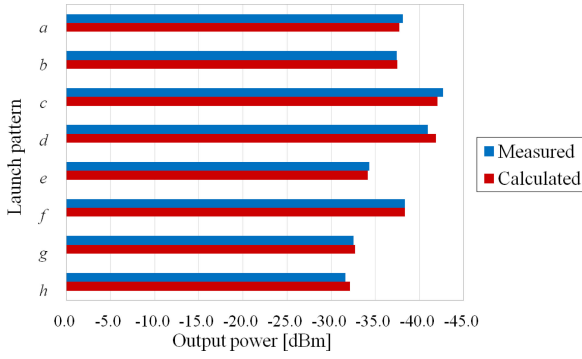


Fig. 15. Output power from channel 4 under various launch conditions, compared to calculated results.

is written as

$$P_4(XT_{N-4})(\text{dBm}) = P_N + XT_{N-4}. \quad (4)$$

Here, we suppose that the crosstalk from multiple channels accumulates linearly. Then, since channels 3 and 5 are both 125- μm apart from channel 4, the output power from channel 4, $P_4(XT_{3-4}, XT_{5-4})$ due to the crosstalk from both channels 3 and 5 could be expressed as

$$P_4(XT_{3-4}, XT_{5-4})(\text{dBm}) = 10 \log [10^{(P_4(XT_{3-4}))} + 10^{(P_4(XT_{5-4}))}]. \quad (5)$$

By applying (5) to the cases of various multiple-core configurations shown in Fig. 14, the output power from channel 4 is calculated and the results are shown in Fig. 15. The calculated results in Fig. 15 show excellent agreement with the measured results, particularly in the two-channel operation cases (case *e* and *f*), and even in the case of four and nine-channel operations (case *g* and *h*). Thus, if we experimentally find the relationship between the crosstalk value and intercore distance by launching just one core, as obtained from Fig. 12(b) and (c), we can estimate the effect of multichannel simultaneous operation on the crosstalk.

H. Influences of Cladding-Mode Elimination

We have investigated the origin of interchannel crosstalk in multimode polymer optical waveguides. In particular, we have focused on the *mode coupling* of propagating modes in two cores and the *mode conversion* from the cladding modes to propagating modes [20]. We have also proposed that the latter one is the dominant factor for the crosstalk in the waveguides with a pitch size larger than tens of microns. That means the optical power leaked from the core remains in the cladding (as cladding modes) and then recouples to the propagating modes in the neighbor core as crosstalk. Therefore, by reducing the cladding mode power, the interchannel crosstalk could also decrease. Actually, the addition of photoabsorptive materials (carbon-black) further decreases the interchannel crosstalk values in GI-core waveguides as described in [22]. In this section, we focus on the effect of cladding-mode elimination.

Normally, the polynorborene-based waveguides fabricated by Sumitomo Bakelite have a structure being sandwiched be-

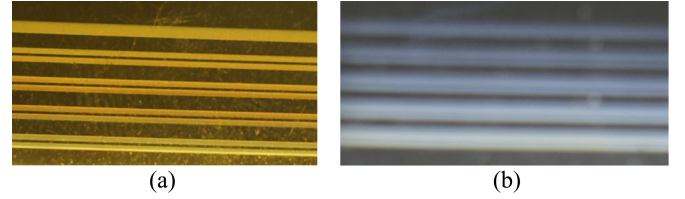


Fig. 16. Photographs of the GI-core waveguides with (a) PI- and (b) no PI-film.

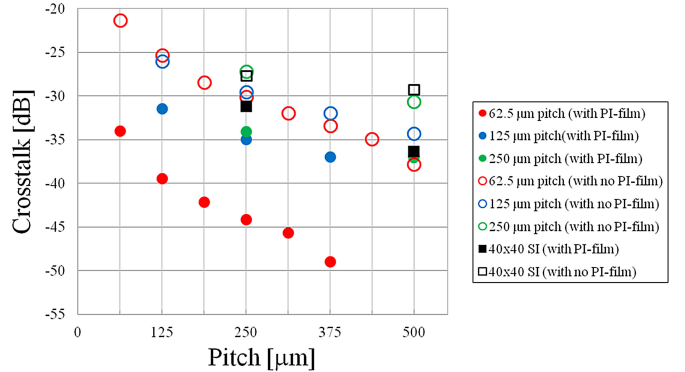


Fig. 17. Interchannel crosstalk measurement results of the GI-core waveguide with and without PI-film having 250-, 125- and 62.5- μm pitches excited via a 50- μm GI-MMF (including the same data shown in Fig. 12).

tween two 25- μm thick polyimide (PI) films for mechanical reinforcement. Actually, most of the GI-square core waveguide samples used in this paper also have the same structure, except for the three samples shown in the crosstalk measurement in Fig. 12 and Table III. The appearances of the waveguides with and without the PI films are shown in Fig. 16: a yellow-color film is visually confirmed in Fig. 16(a). These PI films attached to the cladding could contribute to reduce the cladding mode power, because the refractive index of PI (1.70) is much higher than that of the cladding. Therefore, in this section, we measure the interchannel crosstalk of the GI-square core waveguides with the PI-films in the same way as that shown in Fig. 11. Fig. 17 compares the measured results of the two waveguides: with and without PI-films. Fig. 17 clearly shows the large difference in the interchannel crosstalk of the two waveguides. In particular, approximately 10-dB lower crosstalk is observed in the 62.5- μm pitch waveguide, which is the largest drop in all the waveguides. It is noteworthy that the plots of the crosstalk observed in the 125- μm pitch are located on almost the same line as the plots of the 250- μm pitch waveguide. Contrastingly, little change is observed in the SI-core waveguide even if the PI-films are attached to it. Hence, as we have proposed, interchannel crosstalk in GI-core waveguides is essentially low compared to SI-core waveguides. In particular, less than -30 dB of crosstalk is realized with GI-core waveguides even under a pitch as small as 62.5 μm . Meanwhile, if conditions with remaining high-power cladding modes are realized for whatever reason, high crosstalk is observed, which could be independent of the waveguide structures.

We can conclude that the elimination of the cladding modes strongly contributes to a decrease in the interchannel crosstalk,

TABLE V
CALCULATION RESULTS OF CROSSTALK UNDER MULTICHANNEL OPERATION

ch.	1	2	3	4	5	6	7	8	9	10	11
<i>a</i>	-	-	-	-	0	-34.35	-	-	-	-	-
<i>b</i>	-	-	-	0	0	-32.73	-	-	-	-	-
<i>c</i>	-	-	0	0	0	-32.17	-	-	-	-	-
<i>d</i>	-	0	0	0	0	-31.67	-	-	-	-	-
<i>e</i>	0	0	0	0	0	-31.22	-	-	-	-	-
<i>f</i>	-	-	-	-	0	-31.33	0	-	-	-	-
<i>g</i>	-	-	-	0	0	-29.72	0	0	-	-	-
<i>h</i>	-	-	0	0	0	-29.16	0	0	0	-	-
<i>i</i>	-	0	0	0	0	-28.66	0	0	0	0	-
<i>j</i>	0	0	0	0	0	-28.21	0	0	0	0	0

(dBm).

which is more obvious in GI-core waveguides than SI-core ones, and also in narrower pitch waveguides.

In Table V, we calculate the crosstalk due to multichannel simultaneous operation in the narrowest pitch (62.5- μm) waveguide with PI films, in order to demonstrate how high-density optical wiring is realized with GI-core polymer waveguides. Here, for simplicity, the output power from the excited core(s) is set to be uniform (0 dBm). We use a 12-channel waveguide, so that channels 5 and 6 would show the highest interchannel crosstalk when all the 12 cores are under operation. However, since the PI-films reduce crosstalk, as shown in Fig. 17, the worst crosstalk is still lower than -28 dB, despite 62.5 μm pitch.

IV. GI-CORE WAVEGUIDE CIRCUIT WITH CROSSING STRUCTURES

For realizing high-bandwidth-density O-PCB links, polymer optical waveguide circuits comprised of curved and crossed waveguides, as well as straight ones are expected to be used. In particular, crossed waveguides are strongly anticipated because they realize high-density single-layer optical wirings on PCBs. Therefore, researching crossed polymer waveguides has become more active recently. However, previous studies mainly focus on waveguides with SI-cores, so that the light leakage loss at the crossed core regions [23], [24] has been crucial, because total internal reflection is not caused at the crossed core regions. On the other hand, crossed waveguides composed of GI-cores are also beneficial, because they are capable of reducing those light leakage losses.

The photoaddressing method is a unique and very promising methodology to realize low-loss GI-core crossed waveguides [25], [26]. Actually, we developed GI-square core polymer waveguide circuits including the crossed waveguides as well as bent waveguides, for the first time, to the best of our knowledge. Fig. 18 shows an example of a GI-core polymer waveguide circuit. Detailed properties of the GI-core polymer waveguide circuits will be presented elsewhere.

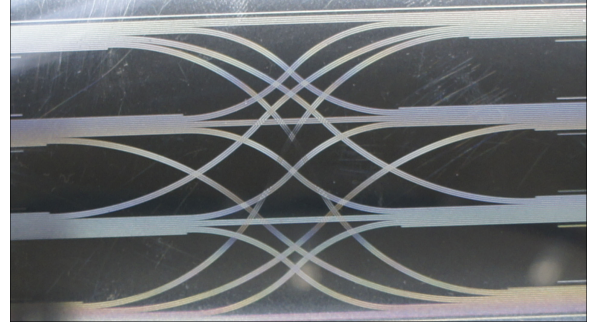


Fig. 18. Top view of a waveguide circuit with crossing structure.

V. CONCLUSION

We introduced a new fabrication method for GI-core polymer optical waveguides: the photoaddressing method. Since the GI-core waveguides are composed of polynorbornene resin with a glass-transition temperature of 250 °C and beyond, we expect that its thermal stability is high enough for O-PCB applications. We experimentally demonstrated that the fabricated GI-core waveguides showed a high connectivity with MMFs widely utilized for off-board interconnects. In addition, low interchannel crosstalk, which should be one of the advantages of GI-core waveguides over their SI-core counterparts were also verified by the fabricated waveguides even under a pitch as narrow as 62.5 μm . We also found a method to estimate the worst-case crosstalk under multichannel operation, and demonstrated that even if 12 channels were simultaneously operated, sufficiently low crosstalk (less than -28 dB) would be maintained in the GI-core polymer waveguide with a 62.5- μm pitch. We believe that the new GI-core polymer optical waveguides will pave the way for realizing low-cost and high-bandwidth-density O-PCBs.

ACKNOWLEDGMENT

The authors would like to acknowledge H. Nasu of Furukawa Electric Co., Ltd. for supplying 50- $\mu\text{m}\phi$ GI-MMF ribbons with variable pitch size, in addition to valuable technical advices.

REFERENCES

- [1] M. A. Taubenblatt, "Optical interconnects for high performance computing," in *Proc. Opt. Fiber Commun. Conf. Expo., Nat. Fiber Opt. Eng. Conf.*, 2011, Paper OThH3.
- [2] M. Tokunari, Y. Tsukada, K. Toriyama, H. Noma, and S. Nakagawa, "High-bandwidth density optical I/O for high-speed logic chip on waveguide-integrated organic carrier," in *Proc. 62nd Electron. Compon. Technol. Conf.*, 2012, pp. 819–822.
- [3] X. Wang, W. Jiang, L. Wang, H. Bi, and R. T. Chen, "Fully embedded board-level optical interconnects from waveguide fabrication to device integration," *J. Lightw. Technol.*, vol. 26, no. 2, pp. 243–250, Jan. 2008.
- [4] R. Dangel, C. Berger, R. Beyeler, L. Dellmann, M. Gmür, R. Hamelin, F. Horst, T. Lamprecht, T. Morf, S. Oggioni, M. Spreafico, and B. J. Offrein, "Polymer-waveguide-based board-level optical interconnect technology for datacom applications," *IEEE Trans. Adv. Packag.*, vol. 31, no. 4, pp. 759–767, Nov. 2008.
- [5] N. Bamiedakis, J. Beals, IV, R. V. Penty, I. H. White, J. V. DeGroot, Jr., and T. V. Clapp, "Cost-effective multimode polymer waveguides for high-speed on-board optical interconnects," *J. Quantum Electron.*, vol. 45, no. 4, pp. 415–424, Apr. 2009.
- [6] F. E. Doany, C. L. Schow, B. G. Lee, R. A. Budd, C. W. Baks, C. K. Tsang, J. U. Knickerbocker, R. Dangel, B. Chan, H. Lin, C. Carver, J. Huang,

- J. Berry, D. Bajkowski, F. Libsch, and J. A. Kash, "Terabit/s-class optical PCB links incorporating 360-Gb/s bidirectional 850 nm parallel optical transceivers," *J. Lightw. Technol.*, vol. 30, no. 4, pp. 560–571, Feb. 2012.
- [7] C. L. Schow, A. V. Rylyakov, C. Baks, F. E. Doany, and J. A. Kash, "25-Gb/s 6.5-pJ/bit 90-nm CMOS-driven multimode optical link," *IEEE Photon. Technol. Lett.*, vol. 24, no. 10, pp. 824–826, May 2012.
- [8] T. Shiraishi, T. Yagisawa, T. Ikeuchi, S. Ide, and K. Tanaka, "Cost-effective low-loss flexible optical engine with microlens-imprinted film for high-speed on-board optical interconnection," in *Proc. 62nd Electron. Compon. Technol. Conf.*, 2012, pp. 1505–1510.
- [9] T. Ishigure and Y. Takeyoshi, "Polymer waveguide with 4-channel graded-index circular cores for parallel optical interconnects," *Opt. Exp.*, vol. 15, no. 9, pp. 5843–5850, Apr. 2007.
- [10] Y. Takeyoshi and T. Ishigure, "High-density 2×4 channel polymer optical waveguide with graded-index circular cores," *J. Lightw. Technol.*, vol. 27, no. 14, pp. 2852–2861, Jul. 2009.
- [11] M. Fujiwara, T. Shirato, H. Owari, K. Watanabe, M. Matsuyama, K. Takahama, T. Mori, K. Miyao, K. Choki, T. Fukushima, T. Tanaka, and M. Koyanagi, "Novel opto-electro printed circuit board with polynorbornene optical waveguide," in *Proc. Int. Conf. Sol. St. Dev. Mat.*, 2006, pp. 840–841.
- [12] K. Soma and T. Ishigure, "Fabrication of a graded-index circular-core polymer parallel optical waveguide using a microdispenser for a high-density optical printed circuit board," *IEEE J. Sel. Top. Quantum Electron.*, vol. 19, no. 2, p. 3600310, Mar./Apr. 2013.
- [13] T. Ishigure and Y. Nitta, "Polymer optical waveguide with multiple graded-index cores for on-board interconnects fabricated using soft-lithography," *Opt. Exp.*, vol. 18, no. 13, pp. 14191–14201, Jun. 2010.
- [14] T. Mori, K. Moriya, K. Kitazoe, S. Takayama, S. Terada, M. Fujiwara, K. Takahama, K. Choki, and T. Ishigure, "Polymer optical waveguide having unique refractive index profiles for ultra high-density interconnection," in *Proc. Opt. Fiber Commun. Conf. Expo. Nat. Fiber Opt. Eng. Conf.*, 2012, Paper OTu11.6.
- [15] Y. Hirobe and T. Ishigure, "Four-channel polymer optical waveguide with W-shaped index profile cores and its low inter-channel crosstalk property," in *Proc. 21st Annu. IEEE Lasers Electro-Opt. Soc. Meet.*, 2008, pp. 443–444.
- [16] H.-H. Hsu, Y. Hirobe, and T. Ishigure, "Fabrication and inter-channel crosstalk analysis of polymer optical waveguides with W-shaped index profile for high-density optical interconnections," *Opt. Exp.*, vol. 19, no. 15, pp. 14018–14030, Jul. 2011.
- [17] F. E. Doany, D. M. Kuchta, A. V. Rylyakov, C. W. Baks, F. Libsch, and C. L. Schow, "Single-chip 4 TX + 4 RX optical module based on holey SiGe transceiver IC," in *Proc. 63rd Electron. Compon. Technol. Conf.*, 2013, pp. 268–273.
- [18] T. Kosugi and T. Ishigure, "Polymer parallel optical waveguide with graded-index rectangular cores and its dispersion analysis," *Opt. Exp.*, vol. 17, no. 18, pp. 15959–15968, Aug. 2009.
- [19] J. B. Schlager, M. J. Hackert, P. Pepeljugoski, and J. Gwinn, "Measurements for enhanced bandwidth performance over 62.5- μ m multimode fiber in short-wavelength local area networks," *J. Lightw. Technol.*, vol. 21, no. 5, pp. 1276–1285, May 2003.
- [20] T. Ishigure, R. Ishiguro, H. Uno, and H.-H. Hsu, "Maximum channel density in multimode optical waveguides for parallel interconnections," in *Proc. 61st Electron. Compon. Technol. Conf.*, 2011, pp. 1847–1851.
- [21] I. Papakonstantinou, D. R. Selviah, K. Wang, R. A. Pitwon, K. Hopkins, and D. Milward, "Optical 8-channel, 10 Gb/s MT pluggable connector alignment technology for precision coupling of laser and photodiode arrays to polymer waveguide arrays for optical board-to-board interconnects," in *Proc. 58th Electron. Compon. Technol. Conf.*, 2008, pp. 1769–1775.
- [22] H. Uno and T. Ishigure, "GI-core polymer parallel optical waveguide with high-loss, carbon-black-doped cladding for extra low inter-channel crosstalk," *Opt. Exp.*, vol. 19, no. 11, pp. 10931–10939, May 2011.
- [23] G. L. Bona, B. J. Offrein, U. Bapst, C. Berger, R. Beyeler, R. Budd, R. Dangel, L. Dellmann, and F. Horst, "Characterization of parallel optical-interconnect waveguides integrated on a printed circuit board," in *Proc. SPIE*, 2004, vol. 5453, pp. 134–141.
- [24] J. Beals, IV, N. Bamiedakis, A. Wonfor, R. V. Penty, I. H. White, J. V. DeGroot, Jr., K. Hueston, T. V. Clapp, and M. Glick, "A terabit capacity passive polymer optical backplane based on a novel meshed waveguide architecture," *Appl. Phys. A: Mater. Sci. Process.*, vol. 95, pp. 983–988, Jun. 2009.
- [25] S. Takayama, K. Moriya, T. Mori, and K. Choki, "Significant reduction of crossing loss using polynorbornene based GI-core optical waveguide," in *Proc. 4th Electron. Syst.-Integr. Technol. Conf.*, 2012, Paper PA-p7.
- [26] T. Ishigure, K. Shitanda, T. Kudo, S. Takayama, T. Mori, K. Moriya, and K. Choki, "Low-loss design and fabrication of multimode polymer optical waveguide circuit with crossings for high-density optical PCB," in *Proc. 63rd Electron. Compon. Technol. Conf.*, 2013, pp. 297–304.

Ryota Kinoshita was born in Shiga, Japan, on June 4, 1989. He received the B.S. degree in applied physics and physicoinformatics from Keio University, Yokohama, Japan, in 2012, where he is currently working toward the M.S. degree in integrated design functions. In April 2014, he will join Sumitomo Bakelite Company, Ltd. His current research interests include evaluation of polymer parallel optical waveguide links toward high-bandwidth-density optical interconnection.

Kimio Moriya was born in Kagawa, Japan, on April 16, 1983. He received the B.A. and M.A. degrees in basic science from the University of Tokyo, Tokyo, Japan, in 2007 and 2009, respectively. He is currently a Researcher at Sumitomo Bakelite Company, Ltd. His current research interest includes on-board optical interconnections realized with multimode polymer optical waveguides.

Koji Choki was born in Yamaguchi, Japan, on July 25, 1964. He received the Bachelor's and Master's degree in chemical engineering from Kyoto University, Kyoto, Japan, in 1988 and 1990, respectively. He is currently the General Manager of Information and Telecommunication Material Laboratories and the Department Manager of Circuitry with Optical Interconnection Business Development Department at Sumitomo Bakelite Company, Ltd. His current research interest includes on-board optical interconnections realized with multimode polymer optical waveguides.

Takaaki Ishigure (M'00) was born in Gifu, Japan, on July 30, 1968. He received the B.S. degree in applied chemistry and the M.S. and Ph.D. degrees in material science from Keio University, Yokohama, Japan, in 1991, 1993, and 1996, respectively. He is currently an Associate Professor at Keio University. In 2005, he was with the Department of Electrical Engineering, Columbia University, New York, NY, USA, as a Visiting Research Scientist. His current research interests include on-board optical interconnections realized with multimode polymer optical waveguides.